



# Methodological comparison of laser stripping solutions with contemporary pulsed lasers for e-drive copper hairpins

Simone D'Arcangelo<sup>1</sup> · Leonardo Caprio<sup>1</sup> · Davide Chesi<sup>2</sup> · Daniele Nocciolini<sup>2</sup> · Rubino Corbinelli<sup>2</sup> · Barbara Previtali<sup>1</sup> · Ali Gökhan Demir<sup>1</sup>

Received: 26 June 2023 / Accepted: 27 October 2023  
© The Author(s) 2023

## Abstract

The electric drives used in traction applications employ conventionally pure Cu bars bent to the required form, inserted in the stator and welded by a laser at the extremities. These extremities, which are referred to as Cu hairpins, should be stripped off from the electrically isolating polymeric enamel. Laser stripping is industrially used to remove the enamel from the Cu surface. Pulsed wave lasers are employed for the purpose with a large variety of solutions industrially available to the end users. The peculiar process may give way to material removal by surface heating for instance using infrared radiation (IR) or ultraviolet (UV) lasers or an indirect material expulsion via near-infrared (NIR) sources. Accordingly all major laser sources, namely CO<sub>2</sub>, active fiber, active disk, and Nd:YAG at different wavelengths, may be used for the purpose. Such laser sources possess very different characteristics regarding the pulse durations, power levels, and beam diameters. As newer laser system solutions are made available, the need for methods and experimental procedures to compare the process performance also increases. This work compares 7 different hairpin stripping solutions based on contemporary pulsed laser sources along with a detailed comparative analysis method. Initially, the 7 laser sources are used for hairpin stripping. The process quality is analyzed through surface morphology, chemistry, and the mechanical strength upon laser welding. Productivity and efficiency indicators are collected. Using the collected data, the work proposes system configurations for three different scenarios prioritizing quality, productivity, and cost.

**Keywords** Electric drives · Hairpins · Laser surface cleaning · Laser paint removal

## List of symbols

$a$	Flange distance mm	$F_{pk}$	Peak load N
$A_{pore}$	Pore area mm <sup>2</sup>	$h$	Hatch distance $\mu\text{m}$
$A_{res}$	Resistant area mm <sup>2</sup>	$h_f$	Frontal height mm
$A_{tot}$	Total area mm <sup>2</sup>	$h_l$	Lateral height mm
$C_c$	Capital cost	$I_c$	Crosshead displacement mm
$d$	Initial crosshead distance mm	MRE	Material removal efficiency cm <sup>3</sup> /min kW
$d_f$	Fiber core diameter $\mu\text{m}$	$N$	Scan loop number
$d_s$	Spot diameter $\mu\text{m}$	$P$	Laser power W
$d_o$	Waist diameter $\mu\text{m}$	$P_{max}$	Max average power W
$f_c$	Collimation length mm	PRR	Pulse repetition rate kHz
$f_f$	Focal length mm	$S_a$	Areal surface roughness $\mu\text{m}$
$F$	Tensile load N	$t$	Enamel thickness mm
		$t_{cycle}$	Cycle time s
		$t_f$	Frontal thickness mm
		$t_t$	Top thickness mm
		$v$	Scan speed m/min
		$w_l$	Lateral width mm
		$w_t$	Top width mm
		$\lambda$	Wavelength nm
		$\varphi$	Porosity %

✉ Ali Gökhan Demir  
aligokhan.demir@polimi.it

<sup>1</sup> Department of Mechanical Engineering, Politecnico di Milano, Via La Masa 1, 20156 Milan, Italy

<sup>2</sup> IMA Automation Atop, Strada S. Appiano 8/A, 50028 Barberino Tavarnelle, Italy

$\bar{\tau}$	Estimated shear strength MPa
$\tau$	Pulse duration ns– $\mu$ s–ms
$\Delta z$	Focal position mm

## 1 Introduction

Contemporary electric drives used in traction systems are based on hairpin windings. The high current density requires large cross-sections and high electric conductivity. Hence, Cu bars are plastically deformed into the required geometry and inserted into the stator to be joint to create the required connection [1]. Conventionally the required joining is carried out through laser welding [2] yet significant challenges remain as indicated [3]. Laser welding provides great flexibility in terms of the used hairpin size and geometry as well as speed thanks to the non-contact process [4]. Industrially laser welding is applied using high power, high brilliance solid state lasers namely the active fiber, and the active disk sources. The joining process is of vital importance as a single stator can comprise up to 200 hairpin couples to be welded. Indeed, for the correct functioning of the stator the hairpin windings are electrically isolated, typically with a polymeric multi-layered enamel. In the production of the stators, the enamel coated Cu bars are stripped from the isolating enamel, cut in the required length, bent, and inserted to the desired position [5]. In the assembled condition the bars stripped from the enamel appear in the form of “hairpins”. The enamel-free regions are accessed by the laser beam for the fusion based welding [6]. Concerning the laser welding of the Cu hairpins, Omlor et al. explored the influence of geometrical deviations of the positioning on the cross-sectional area of the joints [7] whilst Dimatteo et al. investigated the influence of process parameters on the joint properties [8]. Hartung et al. observed the fusion process by means of a camera in order to evaluate the spattering behavior of the melt pool during the laser-material interaction [9]. The output of the laser welding process may be classified via the use of artificial intelligence algorithms as shown by Vater et al. [10] or quantitatively predicted as demonstrated by Mayr et al. [11].

The hairpin stripping process can be industrially carried out by means of cutting tools or with a laser beam. The laser process allows for a contact free process, flexible in terms of the stripped area size and shape. Moreover, the cutting tools may often remove a layer of Cu reducing the effective cross-section of the connection. In all cases, it is desirable to remove a limited extent of the enamel in length to reduce the processing time but also to reduce the consecutive recoating after the laser welding stage [12]. The correct removal of the enamel is essential to avoid laser welding issues due to polymeric material entrapment in the melt pool that can cause porosity, spatter formation, and even

material burst generating several weld flaws [6, 13]. Indeed, several laser sources may be a candidate for the stripping process. As a matter of fact, the process is a variant of laser cleaning or paint removal applied to a limited region of the product in a selective manner [14]. In this process, pulsed wave (PW) lasers are often preferred from ms to ns duration ranges [15]. The paint removal processes can operate in two main ways: (i) direct material removal from the surface if the laser wavelength is sufficiently well absorbed by the polymeric material, or (ii) indirect material removal where the laser is absorbed by the metal at the polymer/metal interface [16–20], where the heating causes shock waves [21] that may expel the material in particles much larger than the beam size [22]. Today, several laser sources, spanning from IR to UV have become commercially available in robust and reliable packages, working as industrial workhorses. The global demand has increased the availability of the laser sources, leading to a significant reduction in the cost per watt (€/W) spent on the sources over the last decade [23]. With such availability of sources, benchmarking works become of great importance both to the scientific communities and the industry. On the other hand, laser sources have often fixed characteristics in terms of available power, pulse duration, pulse repetition rate, and beam sizes. Hence a completely parametric characterization becomes very difficult. Instead, benchmarking through representative solutions of the industrially available sources with an emphasis to the testing criteria and the underlying phenomenon is a viable path. Several works demonstrate the difficulties of welding bare Cu hairpins [24]. To tackle such difficulties advanced machine learning approaches are required for the classification of the output of the welding process as showed by Mayr et al. [11, 25]. Vater et al. demonstrated the use of such approaches for the quality classification of the process [26, 27]. These techniques could be then exploited in an industrial production architecture [28]. Glaessel et al. exposed the influence of process laser welding parameters on the electrical resistance [29] whilst further investigations attempted at correlating this parameter to the re-solidified geometry of the joint [30]. Baader et al. investigated the use of interferometric approaches for in-line monitoring of the joint geometrical characteristics during laser welding [31]. Possibly such data may be exploited to predict penetration depth and provide information on the quality characteristics as shown by Stadter et al. [32]. The use of novel wavelengths for the contacting of the hairpin winding has been explored by Zediker et al. [33]. A comprehensive benchmarking of different laser welding technologies has been provided by the authors in a previous work [34]. On the other hand, the influence of the stripping process on the outcome of the laser welding process has not been investigated in detail.

Accordingly, this work demonstrates the use of 7 different laser system configurations for the stripping of Cu hairpins.

The benchmarked technologies span a large wavelength window from IR to UV, encompassing CO<sub>2</sub>, active fiber, active disk, and Nd:YAG technologies. The stripping quality was evaluated in terms of surface topography and chemistry. In order to evaluate the process performance, stripped hairpin couples were laser welded and mechanically tested through tensile peeling. The results were compared in terms of quality, productivity, and material removal efficiency. The results are used to indicate future laser solutions for this emerging manufacturing process.

## 2 Methodology

The variety of materials, applications, and machining configurations encountered by laser-based manufacturing processes increase rapidly. Laser stripping of hairpins is one application of many that requires a rapid and thorough comparative analysis for the technology choice. In the meanwhile, the number of available laser sources for the application in hand increase in a similarly rapid fashion. Today, laser sources provide flexibility in temporal and spatial beam control as well as wavelength option. The processes employed are difficult to model and simulate, hence, experimental works are required to analyse the quality as well as the final productivity. Often the metrics of performance are

defined through the development of the application. Overall, a comparative analysis of laser systems for a single manufacturing application is a great challenge that requires a methodological approach.

In the specific case of laser hairpin stripping the process and the final stator performance is schematically described in Fig. 1. The laser system removes the enamel, modifying the hairpin surface. The stripped hairpins are laser welded later on. The internal and external defects generated at the end of the fusion based welding process determine the electrical and the mechanical properties. The overall stator performance is directly correlated to this chain of phenomenon. Each passage in this chain provide measurable metrics that are required to analyse the laser stripping quality and productivity. The consequent choice of the laser system has a direct impact on the overall capital and maintenance costs.

Table 1 depicts the measures extractable and quantifiable throughout the hairpin manufacturing cycle. These measures can be directly related to quality, productivity, and cost for the final selection of the laser system. For the comparison of different laser systems used in laser hairpin stripping, the cycle time ( $t_{cycle}$ ) and material removal efficiency (MRE) constitute direct and indirect productivity attributes that can be measured and calculated. At the end of the enamel removal process the surface is modified topographically and chemically, which can be quantified via surface roughness ( $S_a$ ) and chemistry measurements (C content in wt%).

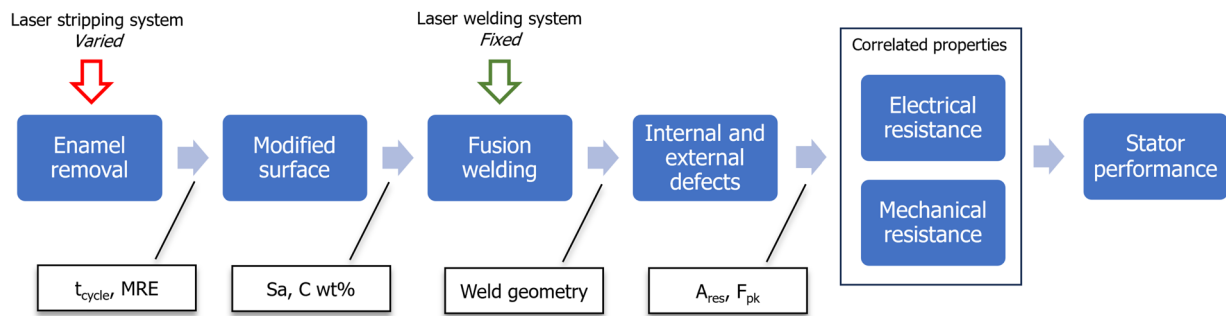


**Fig. 1** The relationship between the laser stripping process and the final stator performance with intermediate effects and measurable quantities in the hairpin manufacturing cycle

**Table 1** Extracted measures and attributes in the hairpin manufacturing cycle

Measure	Attribute	Indicator type	Method
Cycle time	Productivity	Direct	Measured, $t_{cycle}$ [s]
Material removal efficiency	Productivity	Indirect	Calculation, MRE [ $cm^3/min \cdot kW$ ]
Surface roughness	Quality	Indirect	Areal surface roughness, $S_a$ [ $\mu m$ ]
Surface chemistry	Quality	Indirect	Energy-dispersive spectroscopy, C wt%
Mechanical resistance	Quality	Direct	Tensile peel test, $F_{pk}$ [N]
Electrical resistance	Quality	Direct	Not studied
Investment and maintenance	Cost	Direct	Not studied, only indicative

The hairpin couples are then welded, where the weld bead dimensions can vary due to the surface conditions. With a fixed laser welding system, the welded beads have a certain degree of internal and external defects according to the hairpin stripping applied previously. The defects will have an impact on electrical and mechanical properties. In a first approximation, with a larger contact area it can be safely expected that the mechanical resistance of the joint should increase (peak force for failure,  $F_{pk}$ ), and the electrical resistance should decrease. As shown in Table 1 each of these measures can be associated to an adequate analysis method for the required quantification. The cost analysis concerns a wide range of parameters related to the overall production system. In this work, the cost aspects have not been studied, but only shown indicatively in terms of the used laser system. The comparative analysis work has been therefore designed to collect, calculate, and experimentally determine the required measures. Three different scenarios for the final selection have been identified namely: (i) highest quality, (ii) highest productivity, and (iii) reduced capital cost. The collected data was used to allocate the suitable laser system solution each scenario.

### 3 Benchmarking study

#### 3.1 Laser systems

Six different pulsed laser sources were used providing 7 different laser stripping systems for the testing within the benchmarking study. The laser sources provided different wavelengths from IR to UV with pulse durations in the ns regime. Beam shaping capabilities integrated to the sources was also evaluated with the NIR sources. Each system was given a tag as shown in Table 2 for identification throughout the experimental work. A pulsed CO<sub>2</sub> laser operating at 10.6 μm and with 300 W maximum average

power was employed as a conventional solution for polymer processing (IR10). An alternative pulsed CO<sub>2</sub> laser operating at 9 μm wavelength was employed with a 400 W maximum average power (IR9). A pulsed active fiber laser with 50 W average power and 1 μm wavelength was used as a representative case of the conventional ns-pulsed NIR lasers (NIR). An active disk laser operating at a similar wavelength and 2 kW average power was employed with a square shaped beam provided through a dedicated delivery fiber (NIR-BS). A green laser ( $\lambda = 0.532 \mu\text{m}$ ) based with 100 W average power was employed to test a visible wavelength (VIS). This laser was based on an active fiber laser with second harmonic generation and a very high pulse repetition rate at 30 MHz providing a quasi-continuous emission profile. A UV laser operating at 0.355 μm wavelength and 30 W average power was employed as the conventional solution for high precision machining of polymeric materials (UV). Finally, the CO<sub>2</sub> and fiber laser sources were used in series to test a hybrid approach (IR + NIR). In this configuration the aim was to remove the majority of the coating via the IR solution, while the NIR source was employed as a finishing operation to remove the residual layers. After the stripping operations the hairpin couples were laser welded using a 6 kW fiber laser, whose specifications are shown in Table 3.

**Table 3** Main specification of the laser welding system employed

Parameter	Level
Active medium	Active fiber
Wavelength, $\lambda$ [nm]	1070
Max laser power, $P_{max}$ [kW]	6
Fiber core, $d_f$ [ $\mu\text{m}$ ]	100
Collimation length, $f_c$ [mm]	200
Focal length, $f_f$ [mm]	300
Waist diameter, $d_0$ [ $\mu\text{m}$ ]	150

**Table 2** Main specification of the laser systems employed

System	CO <sub>2</sub> 10.6 μm	CO <sub>2</sub> 9.4 μm	Fiber 1.064 μm	Disk 1.030 μm BS	Fiber 0.532 μm	Nd:YAG 0.355 μm	CO <sub>2</sub> + Fiber
Tag	IR10	IR9	NIR	NIR-BS	VIS	UV	IR + NIR
Active medium	CO <sub>2</sub>	CO <sub>2</sub>	Fiber	Disc	Fiber	Nd:YAG	CO <sub>2</sub> + Fiber
Wavelength, $\lambda$ [nm]	10,600	9360	1064	1030	532	355	10,600/1064
Max average power, $P_{max}$ [W]	300	400	50	2000	100	30	300/100
Pulse repetition Rate, PRR [kHz]	< 100	< 200	20–80	5–250	30,000	300	100/100
Pulse duration, $\tau$	2–150 μs	2–800 μs	100 ns	30 ns	1.2 ns	25 ns	2–150 μs; 100 ns
Focal length, $f_f$ [mm]	500	210	100	100	260	250	500/500
Waist diameter, $d_0$ [ $\mu\text{m}$ ]	500	500	39	511 × 511 (square)	39	38	500/50
Capital cost, $C_c$	+	+	+	+++	+++	+++	++

### 3.2 Material

The hairpin material was Cu-ETP with an enamel coating for isolation. The hairpin nominal cross-section was  $3.87 \times 2.66 \text{ mm}^2$  with an effective conductive area of  $9.94 \text{ mm}^2$ . The enamel coating consisted of polyester(amide)(imide) overcoated with poly(amide)(imide) (PAI). The nominal enamel thickness was  $95 \text{ }\mu\text{m}$ . Figure 2 shows the schematic view of the hairpin wire along with a microscope image showing the hairpin/enamel interface.

### 3.3 Experimental conditions

The process parameters for each laser source were settled to fully remove the isolating layer with the fastest process possible. Table 4 shows the final parameter sets determined in previous experimental campaigns that are not reported here for the sake of brevity. In the experiments the lasers were run at the highest power. The spot diameter was chosen as a function of the employed laser source. With the IR10 and IR9 larger beams ( $500 \text{ }\mu\text{m}$ ) were available and consisted of an opportune solution with the high absorptivity available. Similarly with the VIS and UV lasers large beams ( $360\text{--}390 \text{ }\mu\text{m}$ ) were found to be more productive with the high absorptivity of the polymeric material. With the NIR sources smaller beams are needed ( $39\text{--}50 \text{ }\mu\text{m}$ ) to compensate for the low absorptivity of the polymers at this

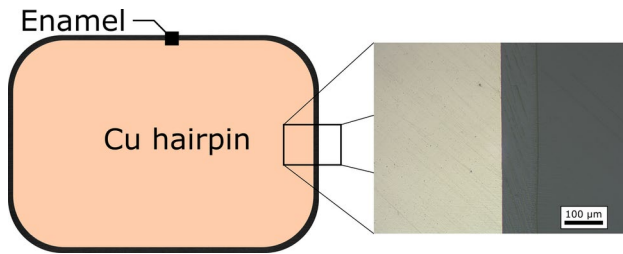


Fig. 2 Cross-section of the Cu hairpin with the enamel

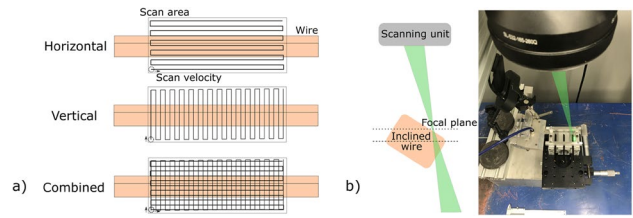


Fig. 3 a Schematic description of the stripping strategies employed. b Specimens during the laser stripping operation

wavelength. The NIR-BS solution compensated for the low absorptivity beam means of a high average power (1 kW) and a relatively large square shaped beam ( $511 \times 511 \text{ }\mu\text{m}$ ). The scan speed ( $v$ ) and the hatch distances ( $h$ ) were adapted as a function of the beam size and the power available. Hatch distance corresponds to the distance between the consecutive laser scan lines, which should be sufficiently small to ensure correct overlap, while higher values provide a faster process. Figure 3a shows the scan strategies studied in the benchmarking work, while Fig. 3b shows the arrangement of the single hairpin under the laser beam. For the benchmarking study different types of scan strategies were found to be adequate between horizontal and vertical ones as well as their combination. The number of passes ( $N$ ) was adapted together with the scan strategy. As a comparison between the different parameter combinations the material removal efficiency (MRE) was calculated using the following equation [20]:

$$MRE = \frac{v \cdot h \cdot t}{N \cdot P} \tag{1}$$

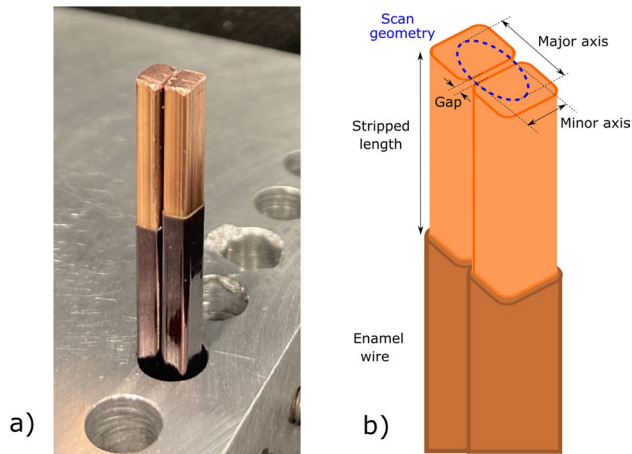
where  $t$  is the enamel thickness,  $P$  is the laser power, and  $N$  is the number of passes. The MRE provides a summary index to how productive a laser beam is per each Watt employed. The index is useful for comparing the efficiency of the beams as well as providing a gross approximation to upscale beam solutions for reducing the process time.

Table 4 Parameter combinations used for each laser system in the benchmarking study

Parameter	IR10	IR9	NIR	NIR-BS	VIS	UV	IR + NIR
Average power, $P$ [W]	300	300	50	1000	100	26	IR: 300; NIR: 100
Focal position, $\Delta z$ [mm]	0	0	0	0	+20	-30	IR: 0; NIR: 0
Spot diameter, $d_s$ [ $\mu\text{m}$ ]	500	500	39	$511 \times 511$ square	390	360	IR:500; NIR: 50
Pulse repetition rate, PRR [kHz]	27	27	50	20	30,000	60	IR: 27; NIR:100
Scan speed, $v$ [m/min]	400	400	120	300	60	60	IR:400; NIR: 240
Scan strategy	Horizontal	Horizontal	Combined	Vertical	Combined	Horizontal	IR: Hor.; NIR: Com
Scan loop, $N$	3	3	3	3	10	2	IR:3; NIR: 3
Hatch, $h$ [ $\mu\text{m}$ ]	50	50	60	500	200	25	IR:50; NIR: 50
Process time for $25 \times 5 \text{ mm}^2$ [s]	0.38	0.38	1.14	0.12	0.63	5.00	IR:0.38; NIR: 0.63
MRE [ $\text{cm}^3/\text{min}\cdot\text{kW}$ ]	2.11	2.11	4.18	1.95	1.14	2.74	IR:2.11; NIR: 3.80

**Table 5** Parameter combinations used for laser welding

Parameter	Value
Laser power, P [kW]	4
Focal position, $\Delta z$ [mm]	+ 1.5
Spot diameter, $d_s$ [ $\mu\text{m}$ ]	215
Scan speed, $v$ [mm/s]	217
Scan strategy	Elliptical
Scan dimensions [mm $\times$ mm]	4.3 $\times$ 2.3
Scan loop, N	5

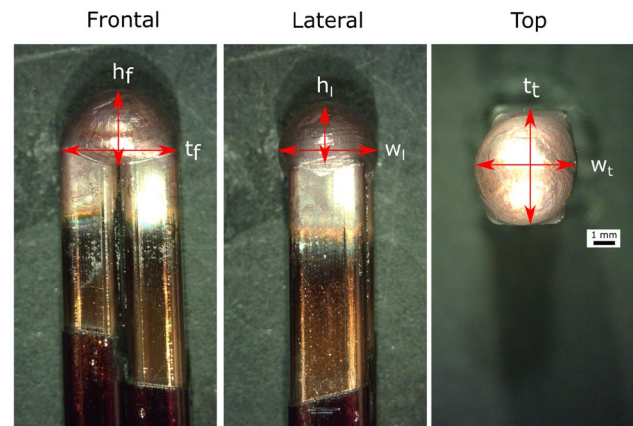
**Fig. 4** a Specimens during the laser welding operation. b Schematic description of the weld scan trajectory

Subsequently, all hairpin couples were welded using the same parameter set in order to test the influence of the stripping quality on the welding operation. The parameter set shown in Table 5 allowed to produce the typical weld bubble in a reasonable process time with sufficient weld penetration ( $> 3$  mm). The hairpins were coupled to have no gap in between as shown in Fig. 4a. An elliptical scan strategy was applied 5 times over the hairpins. For comparison purposes the bare hairpins with no enamel were also welded. A minimum of ten welded specimens were characterized for each condition.

### 3.4 Characterization

#### 3.4.1 Surface morphology and chemistry

Optical microscopy (OM) was employed to characterize the surface appearance after the stripping operations. Scanning electron microscope (SEM) was used to acquire the surface images while energy dispersive spectroscopy (EDS) was used to measure the O and C content due to the remaining enamel on the surface. The measurements by EDS were

**Fig. 5** Schematic description of weld geometry measurements

evaluated in a semi-qualitative manner as the precision of the technique is low for light elements. Focus variation microscopy was employed to acquire the surface profiles and measure the average surface roughness parameter ( $S_a$ ). Once the stripped hairpin couples were welded, the weld morphology was characterized according to Fig. 5 with frontal, lateral, and top side images. The frontal height ( $h_f$ ) and thickness ( $t_f$ ), the lateral height ( $h_l$ ) and width ( $w_l$ ), the top thickness ( $t_t$ ) and width ( $w_t$ ) were measured.

#### 3.4.2 Mechanical characterization

A peel test was conducted to investigate the mechanical integrity of the welded joints. The weld performance is related to the quality of the stripping process that may generate the differences during the welding. For the electric drives the mechanical strength remains the essential requirement as the vibrations and the forces applied may result in the failure of the stator. On the other hand, the mechanical strength is often correlated to the electrical resistance, where often a larger cross-section area provides a stronger joint along with a smaller electrical resistance [30]. Mechanical tests were carried out according to BS EN ISO 14270:2016. Welded samples were bent to achieve a flange length of 15 mm and a crosshead distance of 70 mm using a dedicated bending fixture to form the configuration shown in Fig. 6. The testing velocity was 10 mm/min. The force ( $F$ ) was recorded as a function of the crosshead position ( $l_c$ ). The peak load ( $F_{pk}$ ) was used to assess the strength of the joint.

#### 3.4.3 Fracture surface

The porosity of the fracture surfaces was evaluated to reveal the leading failure mechanism. Figure 7 depicts the measurement of the net area starting from an optical microscopy image of the fracture region. In the analysis

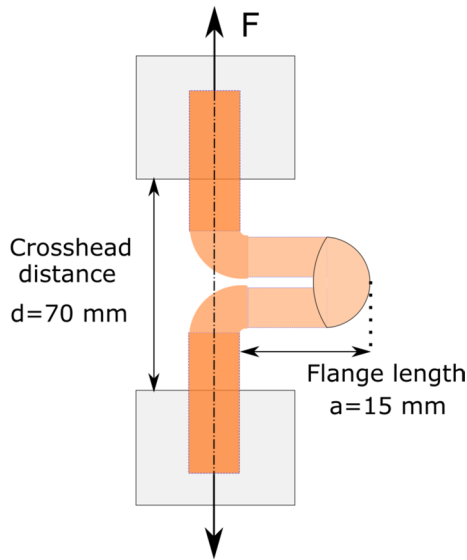
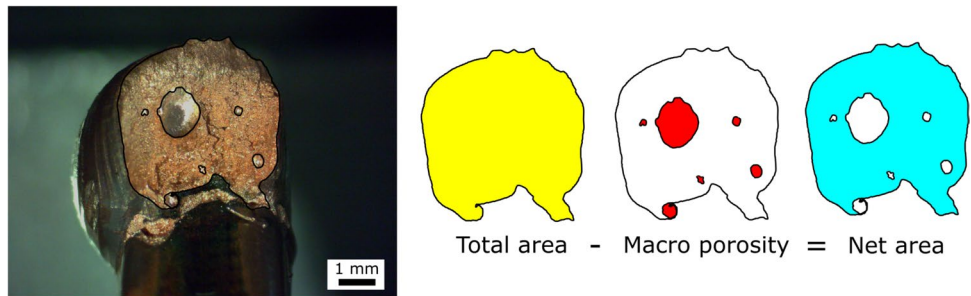


Fig. 6 Schematic description of the mechanical testing configuration

the total area of the fracture surface is measured, and the macro pore areas are subtracted to reveal the effective resistant area ( $A_{res}$ ). This method was chosen over non-destructive analysis via computed tomography scanning, although the latter provides more accurate evaluation on a single specimen through a lengthy measurement procedure. In order to have a one-to-one comparison of the large number of specimens evaluated, the fracture surfaces were measured.

Fig. 7 Schematic description of the porosity and the effective resistant section measurements taken on the fracture surfaces



## 4 Results

### 4.1 Surface topography and roughness after stripping

Figure 8 gather the optical microscopy and SEM images of the surfaces after the stripping operation. It can be seen that the laser types with good absorptivity with polymeric materials provide a smooth surface such as in the case of IR10, IR9, VIS, and UV. The IR wavelengths are not absorbed by the underlying Cu as effectively as for other wavelengths considered, while the VIS and UV wavelengths do not generate further damage below the enamel due to the larger beams decreasing their intensity. The use of NIR provides a roughening of the surface due to the relatively smaller beams and direct ablation of the underlying Cu. In the case of NIR and NIR-BS the surfaces are composed of molten and solidified material, typical of ns-pulsed ablation. A similar effect is present when the IR and NIR solution are employed in a consecutive way. The surface appearance reflects the machining condition provided by the last stripping process applied.

### 4.2 Surface roughness and chemistry

Table 6 shows the average surface roughness ( $S_a$ ), oxygen and carbon content measured on the bare and stripped surfaces. It can be observed that the average surface roughness ( $S_a$ ) range from 2 and 5  $\mu\text{m}$ . Despite smooth looking

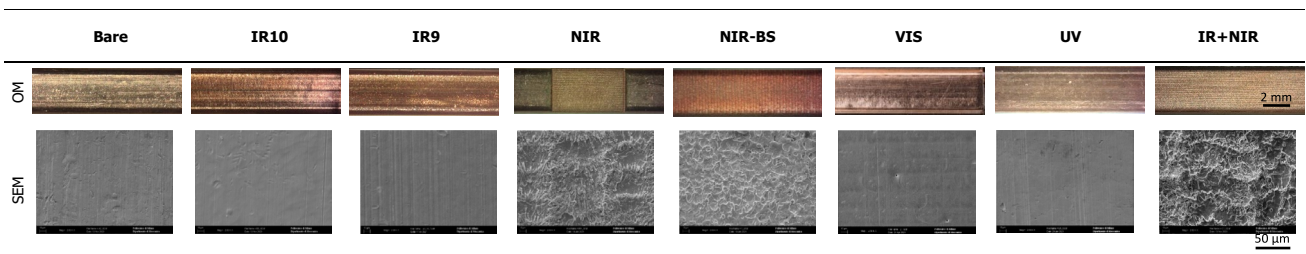


Fig. 8 Optical microscopy and SEM images of the laser stripped hairpins

**Table 6** Surface roughness, carbon, and oxide contents measured on the laser stripped hairpins with different laser sources

	Bare	IR10	IR9	NIR	NIR-BS	VIS	UV	IR + NIR
Sa	2.1 $\mu\text{m}$	4.8 $\mu\text{m}$	2.8 $\mu\text{m}$	3.0 $\mu\text{m}$	1.6 $\mu\text{m}$	3.7 $\mu\text{m}$	5.1 $\mu\text{m}$	2.1 $\mu\text{m}$
C	5.5 $\pm$ 0.6 wt%	48.5 $\pm$ 2.6 wt%	34.7 $\pm$ 1.5 wt%	11.6 $\pm$ 1.1 wt%	10.5 $\pm$ 1.0 wt%	7.9 $\pm$ 2.5 wt%	6.1 $\pm$ 1.0 wt%	4.9 $\pm$ 2.1 wt%
O	0.1 $\pm$ 0.1 wt%	2.6 $\pm$ 0.3 wt%	1.8 $\pm$ 0.3 wt%	4.0 $\pm$ 0.5 wt%	2.8 $\pm$ 0.3 wt%	0.3 $\pm$ 0.2 wt%	0.6 $\pm$ 0.2 wt%	0.9 $\pm$ 0.5 wt%

surfaces, the IR10, IR9, VIS, and UV solution appear to have larger surface roughness values. This is attributed to local variations of the removal behaviour also shown with a larger fraction of O and C content on the surface. On the other hand, the NIR and NIR-BS conditions show an increased surface roughness principally due to the resolidified layers of material. A reduced amount of C is interpreted as lower presence of the polymeric enamel on the surface. The presence of C in the bare hairpin is related to the contaminations from the atmosphere. From this perspective IR + NIR condition appears to provide the most beneficial solution. The oxygen content is relatable both to the presence of the polymeric enamel as well as the oxidation state of the Cu hairpin. Indeed, in all cases the oxygen content remains to be higher than the bare condition.

### 4.3 Bead morphology after laser welding

Figure 9 shows the optical microscopy images of the welded samples corresponding to different stripping conditions. The corresponding geometrical attributes are shown in Fig. 10. In all cases the typical spherical shape of the weld is achieved. Overall sufficient welding depth ( $h_p$ ) at 3 mm has been achieved in all the conditions. The weld morphologies appear slightly different between the conditions. A rounded dome is visible in IR10 and IR9, with differences seen in the  $w_t$  and  $w_l$  measurements. On the other hand, the weld coverage appears to be constant over the experimented condition providing consistent joints with an average value of approximately  $t_f = 5$  mm.

### 4.4 Mechanical resistance of the welded hairpins

Figure 11 shows the tensile test curves of the investigated conditions, where the curve corresponding to the median value of the  $F_{pk}$  is highlighted in red. It can be seen that the peak force is achieved later on followed by reduction of the force prior to the final failure as a typical behaviour. The values of  $F_{pk}$  are variable between 150 and 600 N between the different conditions underlying that the stripping quality has a direct effect on the mechanical behaviour. It can be readily viewed that the combined IR + NIR condition provides the highest  $F_{pk}$  values. Figure 12 shows the fracture surfaces observed by optical microscopy. During the tests, the hairpins failed parallel to the long axis of

the pin couples, rather than the connection zone between the bead and the individual hairpin. This factor confirms the efficacy of the mechanical test to avoid soliciting the connection zones as well as the fact that the weld bead defects are the main cause of the failure. The images in Fig. 12 show that the macro pores with diameters up to 1 mm are formed reducing the resistant area of the weld and are present in all cases. In the case of IR10 the fracture surface has a much rougher appearance accompanied by smaller pores. These small pores are expected to be due to the polymeric gas entrapment during the welding process. Amongst the different conditions, the bare hairpins constitute the enamel-free condition, where the defects are expected to be due to the keyhole pores, spatter formation, and possibly entrapment of the surrounding gas resulting in the pore formation. In the stripped cases, the remaining polymeric enamel is expected to further contribute by the entrapment of the polymeric gasses in the weld bead.

Figure 13 reports the  $F_{pk}$  measured for all the conditions. The bare condition provides an average of 315 N. The IR9, NIR, NIR-BS, UV, and VIS solution provide comparable results as the average value of  $F_{pk}$ . On the other hand, the IR + NIR solution and the IR10 solutions provide significantly different results. The combined process increases  $F_{pk}$  up to 409 N and the single IR10 solution reduces the average value down to 262 N. In order to test the statistical significance of the used laser stripping solution analysis of variance (ANOVA) was used with a statistical significance level of alpha value at 5%. Table 7 depicts the analysis of variance table on the output  $F_{pk}$ . The analysis confirms that the type of laser system used for the stripping process has an impact on the weld strength, as the calculated p-value is lower than 5%. Table 8 reports the Tukey comparisons between the different stripping configurations. The configurations that share the same letter provide statistically the same strength. The combined NIR + IR strategy provides the highest strength. The UV, IR9, NIR, NIR-BS, and VIS conditions provide results that are statistically indifferent and comparable to the bare hairpins. IR10 appears to provide inferior results compared to the bare condition and is statistically similar to IR9, NIR-BS, and VIS. Overall the results show that the combined process provides an enhancement of the

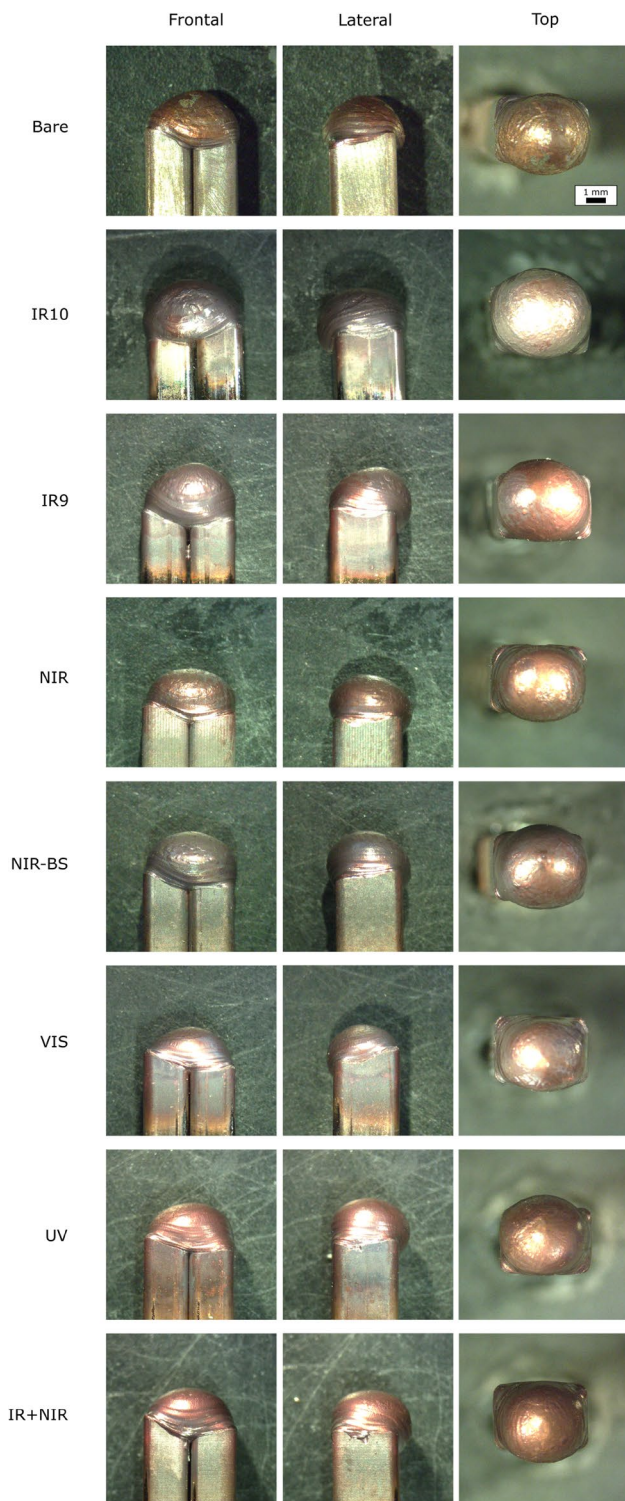


**Fig. 9** Optical microscopy images of laser welded hairpins laser stripped using the different systems

mechanical properties even compared to the bare hairpin without any enamel.

#### 4.5 Porosity measured on the fracture surfaces

Figure 14 shows the porosity levels measured on the different laser stripped conditions. The values have a large discrepancy independently from the laser source type employed with average values between 5 and 15%. The average porosity values do not appear to follow a direct relationship with the mechanical properties. For instance, the average porosity of bare hairpins is similar to that of IR10, which provided the least favorable mechanical properties. The porosity of the UV samples was also high, despite relatively high mechanical properties. This phenomenon indicates that the sole porosity parameter does not provide a sufficient overview to the mechanical properties as the fusion volume also changes with the different stripping conditions.

Figure 15 shows the relationship between the porosity and the effective resistant area with respect to the peak force for failure. It can be seen that the porosity levels are not well correlated to the mechanical strength (Fig. 15a). This is mainly due to the fact that the porosity does not provide sufficient information to the quantity of the resistant area. As the weld bead size and therefore the resistant area varies along with the porosity levels, the use of porosity on its own appears to be insufficient. On the other hand, an increase of the mechanical resistance with the increase of the effective area is confirmed (Fig. 15b). However, the data shows a large dispersion indicating that beyond the resistant area other phenomenon may be contributing to the mechanical resistance. Such factors may be related to the material softening and chemical variations due to the polymeric vapour entrapment. It should also be noted that the resistant area is measured over the fracture surface as a simple projection. The surface and the resistant section are more complex in form. Resultantly the measurement method is expected to induce a certain degree of error too.

A linear regression was fitted to the data in Fig. 15b in the following form:

$$F_{pk} = S_{app}A_{res} \tag{2}$$

where  $S_{app}$  is the apparent strength to the mechanical test with a value of  $31.7 \pm 0.9$  MPa (95% confidence interval for the mean) with  $R^2_{adj}$  at 95.5%. The specimens failed in the vertical direction during the mechanical tests, indicating a shear dominant failure mechanism. Hence, the apparent strength can be interpreted close to the shear strength of the welds. During the tests, the specimens were pulled with an approximate hinge point at the top of the weld bead, while the bottom of the bead could be approximated to the region where the shear moment is applied. These conditions indicate an amplification of 3 to 4 concerning the moment arm generated at the direction where the peel force is applied. Hence, the shear strength can be

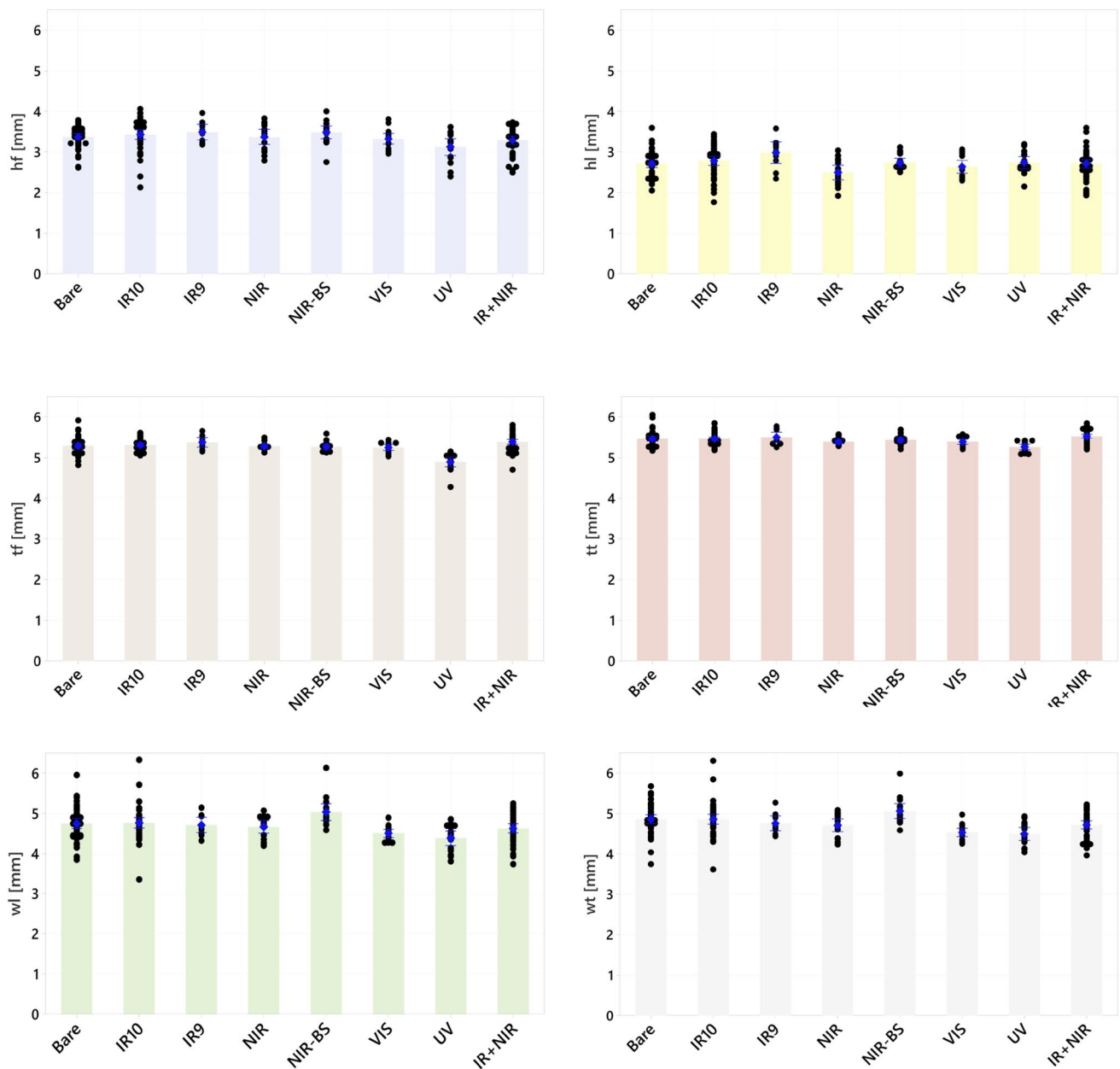


Fig. 10 Bead geometry measurements of laser welded hairpins laser stripped using the different systems

estimated at  $\bar{\tau} = 95\text{--}130$  MPa. The tensile strength of pure Cu is 180–260 MPa with a yield strength at 30–60 MPa [30]. Hence the approximate shear strength would correspond on average 51% of the tensile strength. In literature the welded Cu specimens were observed to have a tensile strength reduction from 180 to 160 MPa [35], while the shear strength of laser welded thin sheets was measured at approximately 180 MPa [36].

## 5 Discussion

### 5.1 Material removal dynamics

The analysis shows that in particular the IR + NIR condition stands out as the one with the lowest average C content providing an increase of the peak force. The UV solution follows with a relatively higher C content and a reduction in the

**Fig. 11** Tensile curves of the laser welded hairpins using the different laser systems. The curve providing the mean value of  $F_{pk}$  is highlighted in red

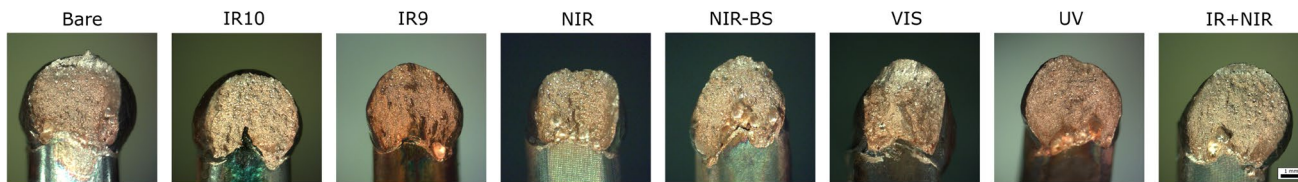
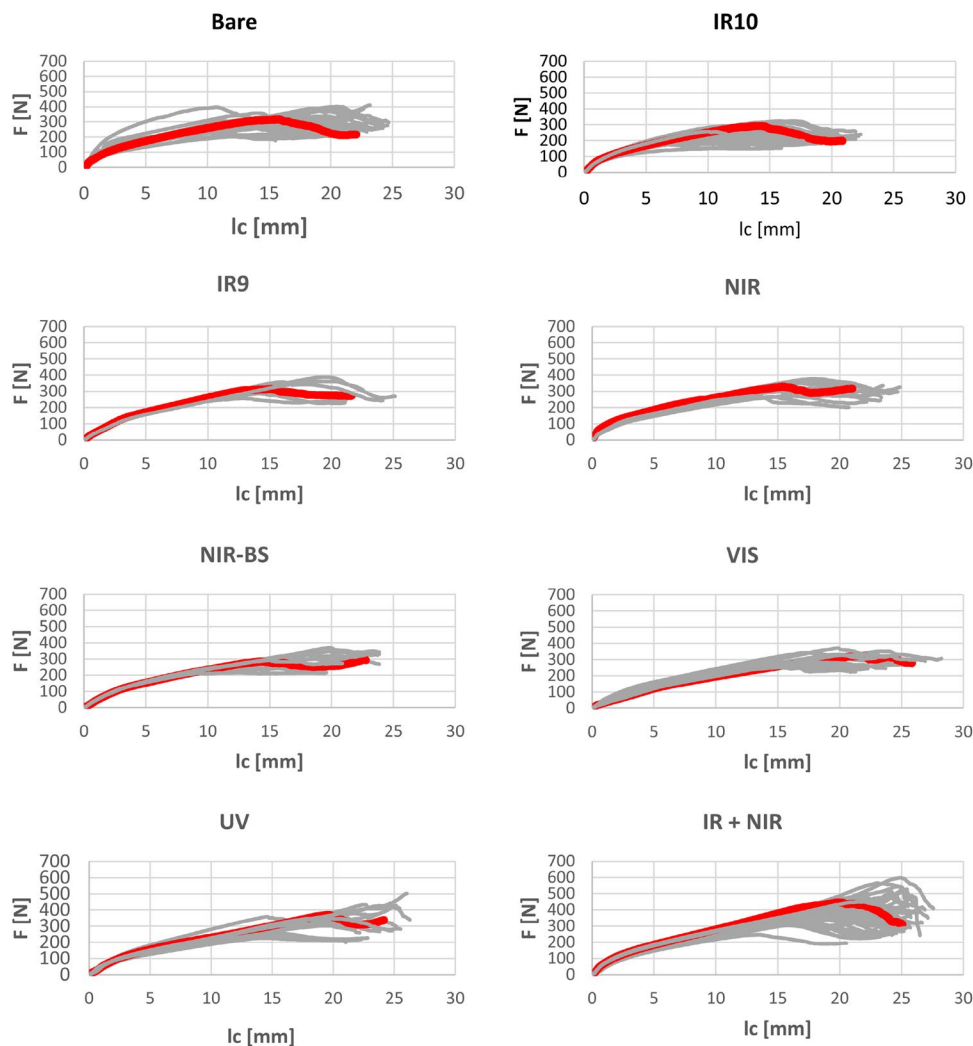


**Fig. 12** Fracture surfaces of the hairpins laser stripped by different systems

mechanical properties. The VIS, NIR-BS, NIR conditions are grouped in a similar range of C content and resistance comparable to the bare hairpin performance. Both IR9 and IR10 have a large content of C that can be the sign of incomplete removal of the enamel remaining at the base coating of polyester(amide)(imide). Evidently, the excess of the polymeric content leads to a significant reduction of the strength.

The welding laser emits at NIR wavelength, which has been shown to effectively interact with the enamel material. However, in the case of the continuous wave (CW) emission of a high-power active fiber laser, the enamel is removed by

a burning process generating fumes and vapor. Such fumes and vapour can be entrapped in the weld seam. Enamel stripping is therefore carried out to eliminate the second material in the melt pool region and beyond. The stripping process has the aim to remove the enamel completely. However, incomplete removal may occur due to the multi-layered structure of the enamel, which may generate differences in the absorptivity. From a basic perspective the  $CO_2$  [17, 37] and the UV [38, 39] lasers are highly suitable for absorption by polymeric materials. The results of the work show that the  $CO_2$  laser may provide sufficient cleaning and

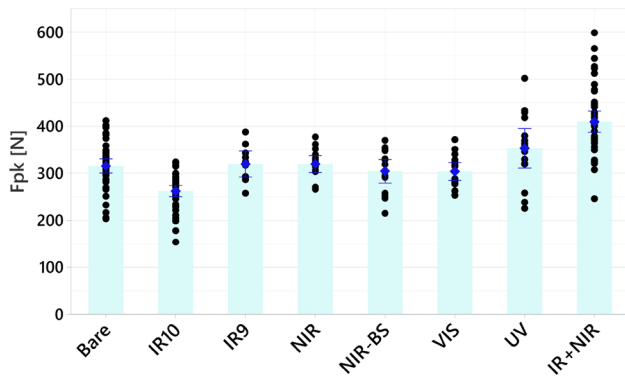


Fig. 13 Peak load of the tested conditions

Table 7 Analysis of variance applied to peak load

Source	DF	Adj SS	Adj MS	F-Value	P-Value
System	7	527,865	75,409	25.60	0.000
Error	197	580,315	2946		
Total	204	1,108,180			

Table 8 Tukey comparisons between the different systems in the increasing order of mechanical average strength from left to right

System	Mean	Grouping
IR + NIR	409	A
UV	353	B
IR9	320	B
NIR	319	B
Bare	315	B
NIR-BS	304	B
VIS	304	B
IR10	262	C

The tested conditions that do not share a letter possess statistically different mechanical properties

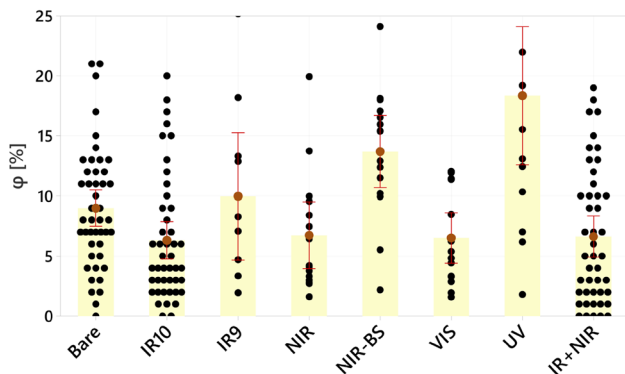


Fig. 14 Porosity levels on the fracture surfaces of the hairpins welded by different systems

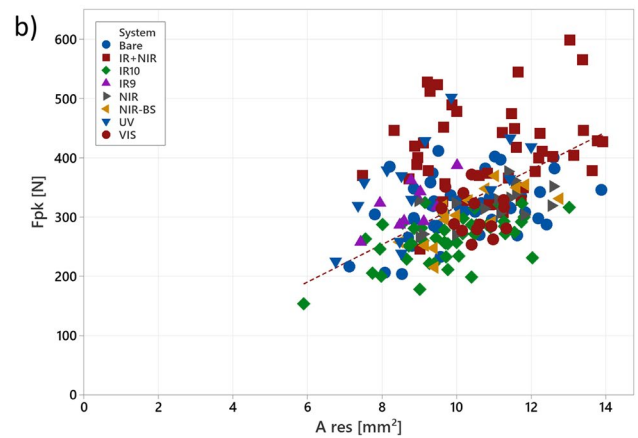
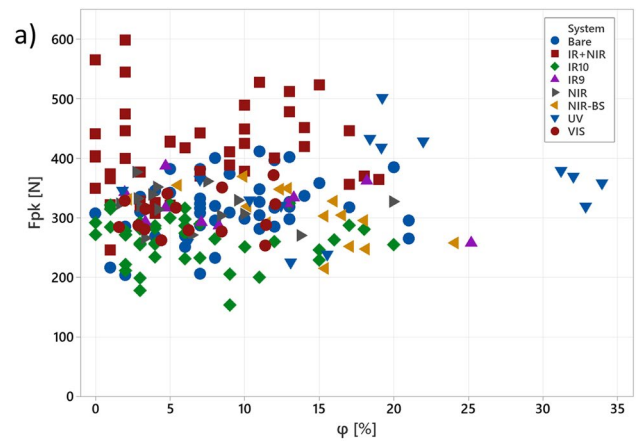


Fig. 15 Correlations between a) the porosity and b) the effective resistant area with respect to the peak load

results comparable to a welding applied to bare hairpins if the process parameters are chosen in an opportune way. This may often lead to a reduction of the process productivity. The UV laser also was found to be highly effective in the enamel removal. The main issue with the UV lasers remains the higher cost and reduced lifetime of the high power UV sources due to the harmonic conversion. Green lasers have also been used for polymeric material removal in an effective way [40]. The VIS laser source provided a good cleaning capacity with results similar to the bare hairpins. The power levels of the VIS laser sources, in particular with green wavelength are rising as also due to the improved absorption of Cu exploitable during the welding operations [41]. Despite its advantages, green lasers are more expensive compared to NIR and IR counterparts. The green wavelength is commonly generated via harmonic conversion starting from a NIR source, increasing also the energy consumption compared to a NIR source with the same power output. The NIR sources on the other hand proved to be highly effective in material removal. The UV, VIS, and IR emissions are expected to be absorbed at the material surface resulting in a direct material removal via ablation, vaporization, and

melt expulsion. In the case of NIR, the laser is expected to generate an indirect material removal by partially being absorbed at the enamel-metal interface. The heated region can expel material in larger particles. Often the underlying Cu surface is machined due this interaction mechanism, as seen in the results. The combined effect of an IR laser followed by a NIR treatment was found to be highly effective. It is expected that the IR laser removes the outer layers of the material leaving partially not removed the inner parts of the multi-layered enamel. The NIR laser is expected to expel the material in an efficient manner. The combined effect results in a cleaner surface with low C contamination and a higher mechanical resistance compared to the bare hairpins. This implies that beyond the chemical contaminant removal the NIR laser treatment can induce secondary effects beneficial for the mechanical resistance. Although not studied in a detailed way in this work, some effects can be hypothesized. The texture induced by the NIR laser may provide better beneficial effects related to the laser beam optical absorption or an enhanced wetting behaviour [42, 43]. Indeed, the provided solution increases the capital cost of the machinery employed.

It should be noted that the enamel isolators are designed for electrical purposes, while their optical and thermal properties are not necessarily matched for a laser-based removal process. Future materials can be potentially optimized for easy removal with a matching industrial laser type.

## 5.2 System selection scenarios

Figure 16 depicts the main direct quality attribute peak force ( $F_{pk}$ ) as a function of the main indirect quality indicator C content, as well as the direct productivity indicator the cycle time and the indirect productivity indicator material removal efficiency (MRE). Figure 16.a shows the relationship between the measured C content and the mechanical resistance of the welded hairpins. The higher presence of C appears to be correlated to a decrease in the mechanical resistance of the welds. For the highest quality scenario, the most suitable solution appears to be IR + NIR. Figure 16.b shows the peak force ( $F_{pk}$ ) as a function of the cycle time. Amongst the available sources, the NIR-BS solution is the most suitable for the highest productivity scenario, with a mechanical resistance comparable to the bare hairpins. The reduced capital cost scenario can be evaluated in a simplistic manner for a compromise between quality and productivity. For this purpose, the conditions that provide a cycle time lower than 1 s and the weld quality comparable to bare condition is required. Accordingly, both the IR10 and IR9 conditions can be taken as appropriate. It should be noted that the cost comparison is based on a simple estimation of the capital required to purchase the laser system. An important cost factor can be associated to the scraps and

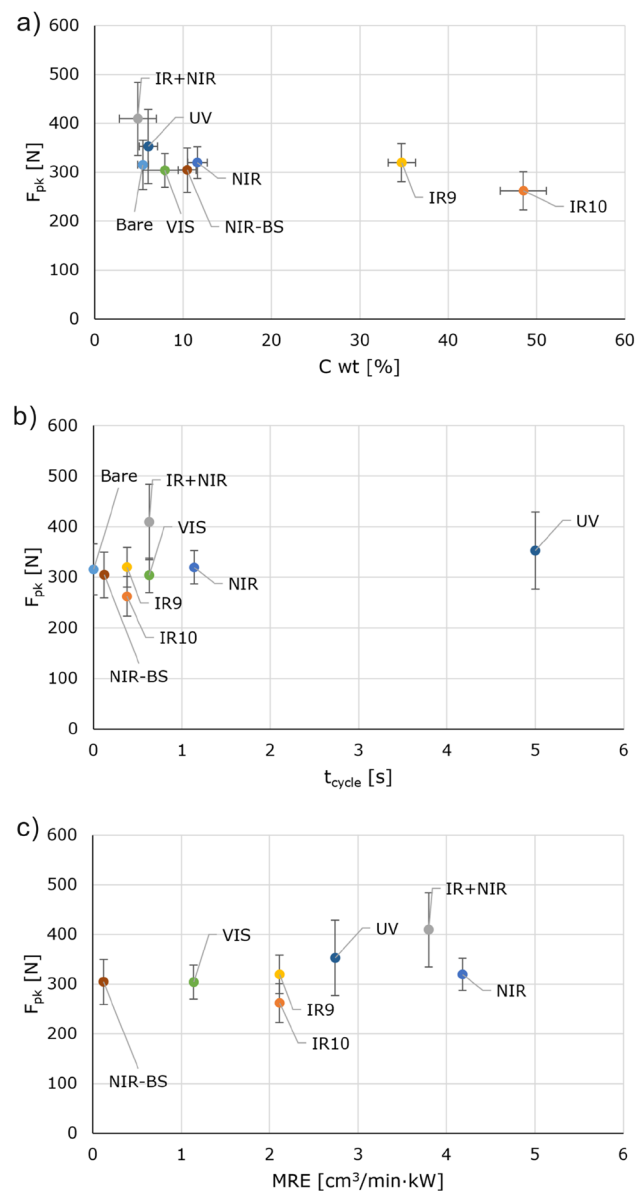


**Fig. 16** Correlation between the peak load and **a** the residual C content, **b** cycle time, and **c** material removal efficiency. Note that “bare” condition has been removed assigned at 0 s cycle time and has been removed in the graph concerning material removal efficiency. The slowest process step in IR + NIR was considered for the cycle time and material removal efficiency. Error bars represent standard deviation

non-conformal parts generated. Such considerations require a wider analysis of the system robustness and the possibility of using in-process monitoring solutions. Table 9 collects the allocated laser system for each scenario.

The material removal efficiency (MRE) can be further evaluated for the development of future laser sources. Figure 16.c shows the peak force against the material removal efficiency for the employed laser systems. According to the analysis, the IR solution can be chosen as the baseline.

**Table 9** Summary of selection scenarios and the possible solutions

Scenario	Criteria	Solution
Highest quality	$\max(F_{pk})$	IR + NIR
Highest productivity	$\min(t_{cycle})$	NIR-BS
Reduced capital cost	$\min(C_c)$ while $(t_{cycle} < 1 \text{ s})$	IR10; IR9

The increased power of VIS lasers should not provide a great advantage. On the other hand, high power UV lasers can essentially be more productive. The 3 different NIR sources used provide a very interesting result in terms of material removal efficiency. The increase of the laser source power results in a decrease from 4.18  $\text{cm}^3/\text{min}\cdot\text{kW}$  at 50 W average power to 3.80  $\text{cm}^3/\text{min}\cdot\text{kW}$  at 100 W and finally to 1.95  $\text{cm}^3/\text{min}\cdot\text{kW}$  at 1000 W. Indeed, the available data is scarce and sparse to draw conclusive interpolations. However, it may be plausible that the higher power levels generate a large quantity of vapour and plume that may shield the laser from effectively reaching the material.

## 6 Conclusions

This work presented a methodological study of laser enamel stripping of Cu hairpin windings. A methodological framework was proposed starting from the phenomenological relationship between the processes and the product performance. For quality and productivity measures and related methods were identified. In the comparative analysis, a total of 7 different laser systems were tested encompassing wavelengths from IR to UV with different pulse durations and beam sizes. The benchmarking work showed the analysis criteria in a wide range of process parameters that were hard to study in a parametric way across the different laser systems. The results showed that the functional testing of the stripping operation through the mechanical strength of the welded joints is an effective way. The results depict that the surface cleanliness plays a direct role on the welded joint strength, while secondary effects related to surface topography may play a role to further enhance the strength. The entrapment of the polymeric vapour in the weld bead reduced the effective area. From the tested solutions the combined use of a  $\text{CO}_2$  and a fiber laser was found to provide the strongest joints. Such solution may require bigger investment costs, however, this is expected further decay due to the decreasing costs of the lasers. On the other hand, several solutions namely  $\text{CO}_2$ , fiber, green, and UV lasers provided comparable results to bare welded Cu hairpins. The main difference lay in terms of the process efficiency, where the fiber lasers appeared to be beneficial for further development of the systems. In the identified scenarios the use of combined NIR + IR was found

to be the most suitable for quality, while the high power NIR-BS source was found to be the most productive. While the present work showed a main quality parameter related to static tensile peel testing, the defect types and morphologies may have different effects on the fatigue properties. Future works will expand the studies over a wider range of component characteristics towards functional tests.

**Funding** Open access funding provided by Politecnico di Milano within the CRUI-CARE Agreement.

**Data availability** The data will be provided upon reasonable request.

## Declarations

**Conflict of interest** The authors declare that they have no conflict of interest.

**Open Access** This article is licensed under a Creative Commons Attribution 4.0 International License, which permits use, sharing, adaptation, distribution and reproduction in any medium or format, as long as you give appropriate credit to the original author(s) and the source, provide a link to the Creative Commons licence, and indicate if changes were made. The images or other third party material in this article are included in the article's Creative Commons licence, unless indicated otherwise in a credit line to the material. If material is not included in the article's Creative Commons licence and your intended use is not permitted by statutory regulation or exceeds the permitted use, you will need to obtain permission directly from the copyright holder. To view a copy of this licence, visit <http://creativecommons.org/licenses/by/4.0/>.

## References

- Glaessel T, Pinhal DB, Masuch M, Gerling D, Franke J (2019) Manufacturing influences on the motor performance of traction drives with hairpin winding, 2019 9th International Electric Drives Production Conference, EDPC 2019 - Proceedings. <https://doi.org/10.1109/EDPC48408.2019.9011872>.
- Kampker A, Kreisköther KD, Büning MK, Treichel P (2018) Challenge of hairpin technology technology boost for OEMs and plant manufacturers. *ATZelextronik Worldw* 13:54–59. <https://doi.org/10.1007/s38314-018-0068-z>
- Seefried J, Mahr A, Weigelt M, Kühl A, Franke J (2021) Challenges of Contacting Processes for Thin Copper Flat Wires in the Context of Electromechanical Engineering, 2021 11th International Electric Drives Production Conference, EDPC 2021-Proceedings. <https://doi.org/10.1109/EDPC53547.2021.9684202>.
- Arzillo A, Braglia P, Nuzzo S, Barater D, Franceschini G, Gerada D, Gerada C (2020) Challenges and Future opportunities of Hairpin Technologies, IEEE International Symposium on Industrial Electronics. 2020-June 277–282. <https://doi.org/10.1109/ISIE45063.2020.9152417>
- Glaessel T, Seefried J, Kuehl A, Franke J (2020) Skinning of insulated copper wires within the production chain of hairpin windings for electric traction drives. *Int J Mech Eng Robot Res* 9:163–169. <https://doi.org/10.18178/ijmerr.9.2.163-169>
- Bocksrocker O, Speker N, Beranek M, Hesse T (2019) Reduction of spatters and pores in laser welding of copper hairpins using two superimposed laser beams, Lasers in Manufacturing Conference 2019 Reduction. 1–8

7. Omlor M, Seitz N, Butzmann T, Petrich T, Gräf R, Hesse AC, Dilger K (2023) Quality characteristics and analysis of input parameters on laser beam welding of hairpin windings in electric drives. *Weld World* 67:1491–1508. <https://doi.org/10.1007/s40194-023-01500-y>
8. Dimatteo V, Ascari A, Faverzani P, Poggio L, Fortunato A (2021) The effect of process parameters on the morphology, mechanical strength and electrical resistance of CW laser-welded pure copper hairpins. *J Manuf Process* 62:450–457. <https://doi.org/10.1016/j.jmapro.2020.12.018>
9. Hartung J, Jahn A, Bocksrocker O, Heizmann M (2021) Camera-based in-process quality measurement of hairpin welding. *Appl Sci* 11:10375. <https://doi.org/10.3390/app112110375>
10. Vater J, Pollach M, Lenz C, Winkle D, Knoll A, Knoll A (2020) Quality Control and Fault Classification of Laser Welded Hairpins in Electrical Motors, 1377–1381
11. Mayr A, Hauck L, Meiners M, Franke J (2020) Prediction of the Joint Cross-Section of Laser-Welded Hairpin Windings Based on 2D Image Data Using Convolutional Neural Networks, 2020 10th International Electric Drives Production Conference, EDPC 2020 - Proceedings. <https://doi.org/10.1109/EDPC51184.2020.9388193>.
12. Riedel A, Hahn R, Kuehl A, Franke J (2021) Evaluation of different methods for removing the conductor insulation of stranded conductors. *Int Symp Adv Top Electr Eng ATEE*. <https://doi.org/10.1109/ATEE52255.2021.9425036>
13. Glaessel T, Riedel A, Franke J, Kuehl (2022) A Influence of Enameled Wire Preparation on the Laser welding of Hairpin Windings, Electrical Contacts, Proceedings of the Annual Holm Conference on Electrical Contacts. <https://doi.org/10.1109/HLM54538.2022.9969767>
14. . Steen WM, Mazumder J (2010) Laser Material Processing. <https://doi.org/10.1007/978-1-84996-062-5>
15. Li X, Wang H, Yu W, Wang L, Wang D, Cheng H, Wang L (2021) Laser paint stripping strategy in engineering application: a systematic review. *Optik* 241:167036. <https://doi.org/10.1016/j.jlco.2021.167036>
16. Barletta M, Gisario A, Tagliaferri V (2006) Advance in paint stripping from aluminium substrates. *J Mater Process Technol* 173:232–239. <https://doi.org/10.1016/j.jmatprotec.2005.11.029>
17. Kumar M, Bhargava P, Biswas AK, Sahu S, Mandloi V, Ittoop MO, Khattak BQ, Tiwari MK, Kukreja LM (2013) Epoxy-paint stripping using TEA CO 2 laser: determination of threshold fluence and the process parameters. *Opt Laser Technol* 46:29–36. <https://doi.org/10.1016/j.optlastec.2012.04.021>
18. Kuang Z, Guo W, Li J, Jin Y, Qian D, Ouyang J, Fu L, Fearon E, Hardacre R, Liu Z, Li L (2019) Nanosecond fibre laser paint stripping with suppression of flames and sparks. *J Mater Process Technol* 266:474–483. <https://doi.org/10.1016/j.jmatprotec.2018.11.028>
19. Gu J, Su X, Jin Y, Li W, Zeng Z, Zhang D, Xu J, Guo B (2023) Towards low-temperature laser paint stripping by photochemical mechanism on CFRP substrates. *J Manuf Process* 85:272–280. <https://doi.org/10.1016/j.jmapro.2022.11.041>
20. Jasim HA, Demir AG, Previtali B, Taha ZA (2017) Process development and monitoring in stripping of a highly transparent polymeric paint with ns-pulsed fiber laser. *Opt Laser Technol* 93:60–66. <https://doi.org/10.1016/j.optlastec.2017.01.031>
21. Razab MKAA, Mohamed Noor A, Suhaimi Jaafar M, Abdullah NH, Suhaimi FM, Mohamed M, Adam N (2018) A review of incorporating Nd:YAG laser cleaning principal in automotive industry. *J Radiat Res Appl Sci* 11:393–402. <https://doi.org/10.1016/j.jrras.2018.08.002>
22. Roberts DE (2004) Pulsed laser coating removal by detachment and ejection. *Appl Phys A Mater Sci Process* 79:1067–1070. <https://doi.org/10.1007/s00339-004-2632-z>
23. Mayer A (2022) The global market for industrial lasers and laser systems. *Laser Focus World*. 7–13
24. Kuehl A (2022) Effects of Insulation Residues on the Contacting Process of Copper Flat Wire Connections, Electrical Contacts, Proceedings of the Annual Holm Conference on Electrical Contacts. <https://doi.org/10.1109/HLM54538.2022.9969811>
25. Mayr A, Lutz B, Weigelt M, Gläbel T, Kißkalt D, Masuch M, Riedel A, Franke J (2019) Evaluation of Machine Learning for Quality Monitoring of Laser Welding Using the Example of the Contacting of Hairpin Windings, 2018 8th International Electric Drives Production Conference, EDPC 2018 - Proceedings. <https://doi.org/10.1109/EDPC.2018.8658346>
26. Vater J, Schamberger P, Knoll A, Winkle D (2019) Winkle, Fault classification and correction based on convolutional neural networks exemplified by laser welding of hairpin windings, 2019 9th International Electric Drives Production Conference, EDPC 2019 - Proceedings. <https://doi.org/10.1109/EDPC48408.2019.9012044>
27. Vater J, Kirschning M, Scheurenberg D, Abel D, Knoll A (2020) Development of a Cloud- And Edge-Architecture for adaptive model weight optimization of a CNN exemplified by optical detection of hairpin welding, 2020 10th International Electric Drives Production Conference, EDPC 2020 - Proceedings. <https://doi.org/10.1109/EDPC51184.2020.9388192>
28. Vater J, Schlaak P, Knoll A (2020) A modular edge-/cloud-solution for automated error detection of industrial hairpin weldings using convolutional neural networks, proceedings - 2020 IEEE 44th annual computers. *Softw Appl Conf COMPSAC 2020:505–510*. <https://doi.org/10.1109/COMPSAC48688.2020.0-202>
29. Glaessel T, Baat F, Schwinghammer D, Seefried J, Kuehl A, Franke J (2018) Infrared laser based contacting of bar-wound windings in the field of electric drives production. *Proced CIRP*. <https://doi.org/10.1016/j.procir.2018.08.005>
30. Glaessel T, Seefried J, Masuch M, Riedel A, Mayr A, Kuehl A, Franke J (2019) Process Reliable Laser Welding of Hairpin Windings for Automotive Traction Drives, 2019 International Conference on Engineering, Science, and Industrial Applications, ICESI 2019. 1–6. <https://doi.org/10.1109/ICESI.2019.8863004>
31. Baader M, Mayr A, Raffin T, Selzam J, Kühl A, Franke J (2021) Potentials of Optical Coherence Tomography for Process Monitoring in Laser Welding of Hairpin Windings, in: 2021 11th International Electric Drives Production Conference (EDPC), pp. 1–10. <https://doi.org/10.1109/edpc53547.2021.9684210>
32. Stadter C, Schmoeller M, von Rhein L, Zaeh MF (2020) Real-time prediction of quality characteristics in laser beam welding using optical coherence tomography and machine learning. *J Laser Appl* 32:022046. <https://doi.org/10.2351/7.0000077>
33. Zediker MS, Fritz RD, Finuf MJ, Pelaprat JM (2020) Laser welding components for electric vehicles with a high-power blue laser system. *J Laser Appl* 32:022038. <https://doi.org/10.2351/7.0000054>
34. D’Arcangelo S, Caprio L, Chesi D, Nocciolini D, Corbinelli R, Previtali B, Demir AG (2024) Comprehensive benchmarking of laser welding technologies including novel beam shapes and wavelengths for e-drive copper hairpins. *Opt Laser Technol* 169:109964. <https://doi.org/10.1016/j.optlastec.2023.109964>
35. Chen HC, Bi G, Nai MLS, Wei J (2015) Enhanced welding efficiency in laser welding of highly reflective pure copper. *J Mater Process Technol* 216:287–293. <https://doi.org/10.1016/j.jmatprotec.2014.09.020>
36. Eisenreich N, Aeckerle M, Bantel C, Heider A, Olowinsky A (2019) Influence of laser parameters on tensile shear strength of copper welds. *J Laser Appl* 31:022411. <https://doi.org/10.2351/1.5096094>

37. Naithani S, Grisard A, Schaubroeck D, Lallier E, Van Steenberge G (2014) Mid-infrared resonant ablation of PMMA. *J Laser Micro Nanoeng* 9:147–152. <https://doi.org/10.2961/jlmn.2014.02.0013>
38. Yung WKC, Liu JS, Man HC, Yue TM (2000) 355 nm Nd:YAG laser ablation of polyimide and its thermal effect. *J Mater Process Technol* 101:306–311. [https://doi.org/10.1016/S0924-0136\(00\)00467-2](https://doi.org/10.1016/S0924-0136(00)00467-2)
39. Lippert T (2005) Interaction of photons with polymers: From surface modification to ablation. *Plasma Process Polym* 2:525–546. <https://doi.org/10.1002/ppap.200500036>
40. Brygo F, Dutouquet C, Le Guern F, Oltra R, Semerok A, Weulersse JM (2006) Laser fluence, repetition rate and pulse duration effects on paint ablation. *Appl Surf Sci* 252:2131–2138. <https://doi.org/10.1016/j.apsusc.2005.02.143>
41. Singh A, Caprio L, Previtali B, Demir AG (2022) Processability of pure Cu by LPBF using a ns-pulsed green fiber laser. *Opt Laser Technol* 154:10831. <https://doi.org/10.1016/j.optlastec.2022.108310>
42. Baumann R, Hipp D, Lasagni AF, Mahrle A (2021) Tailored absorptivity: Increasing the laser weldability of copper through surface structuring. *Mater Lett* 283:128700. <https://doi.org/10.1016/j.matlet.2020.128700>
43. Baumann R, Milles S, Leupolt B, Kleber S, Dahms J, Lasagni AF (2021) Tailored wetting of copper using precise nanosecond direct laser interference patterning. *Opt Lasers Eng* 137:106364. <https://doi.org/10.1016/j.optlaseng.2020.106364>

**Publisher's Note** Springer Nature remains neutral with regard to jurisdictional claims in published maps and institutional affiliations.